research papers

Compressibility of the nitridosilicate SrYb[Si$_4$N$_7$] and the oxonitridoaluminosilicates MYb[Si$_{4-x}$Al$_x$O$_x$N$_{7-x}$] (x = 2; M = Sr, Ba)

E. A. Juarez-Arellano,[a]*
A. Friedrich,[a] **K. Knorr,**[b] **A. Lieb,**[c]
B. Winkler,[a] **M. Amboage,**[d]
M. Hanfland[d] **and W. Schnick**[c]

[a]Institut für Geowissenschaften, Abt. Kristallographie, Johann Wolfgang Goethe-Universität Frankfurt, Senckenberganlage 30, D-60325 Frankfurt a.M., Germany, [b]Institut für Geowissenschaften, Mineralogie, Kristallographie, Christian-Albrechts-Universität zu Kiel, Olshausenstraße 40, D-24098 Kiel, Germany, [c]Department Chemie und Biochemie, Lehrstuhl für Anorganische Festkörperchemie, Ludwig-Maximilians-Universität München, Butenandtstraße 5-13 (D), D-81377 München, Germany, and [d]European Synchrotron Radiation Facility (ESRF), BP 220, F-38043 Grenoble CEDEX, France

Correspondence e-mail:
arellano@kristall.uni-frankfurt.de

The compressibilities of the nitridosilicate SrYb[Si$_4$N$_7$] and the oxonitridoaluminosilicates MYb[Si$_{4-x}$Al$_x$O$_x$N$_{7-x}$] (x = 2; M = Sr, Ba) were investigated by *in situ* high-pressure X-ray powder diffraction. Pressures up to 42 GPa were generated using the diamond–anvil cell technique. The title compounds are structurally stable to the highest pressure obtained. A fit of a third-order Birch–Murnaghan equation-of-state to the p–V data results in V_0 = 302.91 (6) Å^3, B_0 = 176 (2) GPa and B' = 4.4 (2) for SrYb[Si$_4$N$_7$]; V_0 = 310.4 (1) Å^3, B_0 = 161 (2) GPa and B' = 4.6 (2) for SrYb[Si$_{4-x}$Al$_x$O$_x$N$_{7-x}$]; and V_0 = 317.3 (5) Å^3, B_0 = 168 (2) GPa and B' = 4.7 (2) for BaYb[Si$_{4-x}$Al$_x$O$_x$N$_{7-x}$]. While the linear compressibilities of the a and c axes of BaYb[Si$_{4-x}$Al$_x$O$_x$N$_{7-x}$] are very similar up to 30 GPa, distinct differences were observed for SrYb[Si$_4$N$_7$] and SrYb[Si$_{4-x}$Al$_x$O$_x$N$_{7-x}$], with the c axis being the most compressible axis. In all of the investigated compounds the bulk compressibility is dominated by the compression behaviour of the tetrahedral network, while the size of the substituted cation plays a minor role.
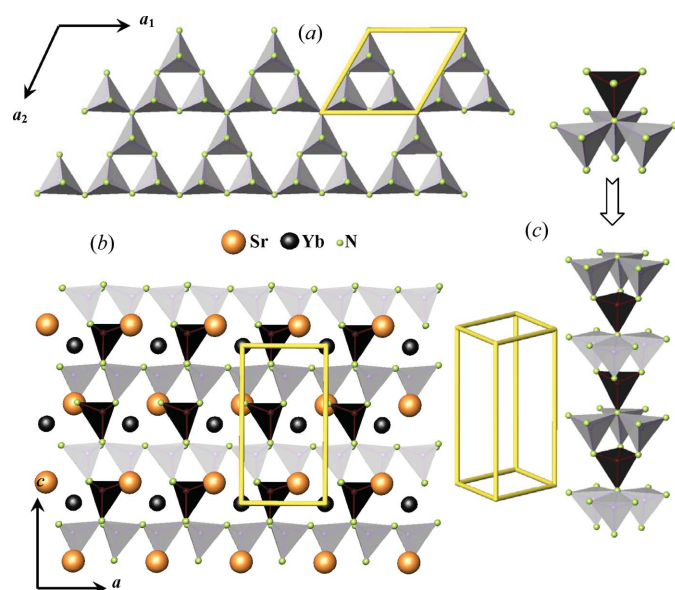
1. Introduction

Nitridosilicates and oxonitridoaluminosilicates are of considerable interest as inorganic materials for high-performance applications owing to their high mechanical hardness and strength, their exceptional thermal and chemical stability and their low density compared with metals (Lauterbach *et al.*, 2000; Schnick *et al.*, 1999; Schnick, 1993). The use of these materials has been reported in different fields and applications, from the production of cutting tools to water-lubricated ceramic tribocomponents with a high potential for engineering applications such as journal bearings, mechanical face seals for pumps and high-pressure fuel injection pumps (Haviar *et al.*, 1997; Amutha Rani *et al.*, 2005; Häntsche & Spicher, 2005).

In comparison with oxosilicates, where Si is fourfold- or sixfold-coordinated by O atoms, in nitridosilicates the Si is surrounded by N atoms, forming SiN$_4$ tetrahedra or SiN$_6$ octahedra. A further partial substitution of Si by Al leads to the oxonitridoaluminosilicates ('sialons'; Schnick, 2001). The first sialons were synthesized by the reaction of Si$_3$N$_4$ and Al$_2$O$_3$ and these compounds were called α- or β-sialons because of their structural similarity to α- or β-Si$_3$N$_4$, respectively (Jack & Wilson, 1972).

The MYb[Si$_{4-x}$Al$_x$O$_x$N$_{7-x}$] (x = 2; M = Sr, Ba; henceforth abbreviated as SrYb- and BaYb-sialon, respectively) compounds are isotypic with the SrYb[Si$_4$N$_7$] nitridosilicate, which crystallizes in the space group $P6_3mc$ (No. 186) with unit-cell parameters a = 5.9880 (3), c = 9.7499 (9) Å, V = 302.76 (2) Å^3 and Z = 2 (Huppertz & Schnick, 1997*a*). Commencing from the SrYb[Si$_4$N$_7$] structure, two Si^{4+} and

N^{3-} ions are replaced by two Al^{3+} and O^{2-} ions, respectively, changing the composition from a nitridosilicate to a sialon without changing the crystal structure. In the $SrYb[Si_4N_7]$ structure the N atoms form a slightly distorted hexagonal dense packing (h.c.p.), where the B layers are occupied by 2/3 in the AB stacking sequence. The tetrahedral voids are occupied by Si atoms in alternating layers having 3/8 and 1/8 occupancies (Fig. 1). Hence, sheets consisting of corner-connected three-membered rings of SiN_4 tetrahedra are formed perpendicular to the c axis (Fig. 1a). These layers are corner-connected along [001] *via* further SiN_4 tetrahedra situated in the less-occupied (1/8) layers (Fig. 1b). The apex N atoms of these tetrahedra are coordinated by four silicon atoms, forming $N^{[4]}$ bridges. In the less-occupied layers, Si_6N_6 rings form channels which contain the M^{2+} and Yb^{3+} cations (Fig. 1b). The M^{2+} and Yb^{3+} ions are found in anticuboctahedral and octahedral coordination, respectively. Alternatively, the structure can be described by star-shaped $[N(SiN_3)_4]$ building blocks (Fig. 1c), where the central $N^{[4]}$ atoms simultaneously bridge four Si tetrahedral centres. These building blocks are connected through common $N^{[2]}$ atoms (Figs. 1b and c).

Only in recent times have the related nitridocarbidosilicates and oxonitridosilicate chloride compounds been investigated experimentally at high pressure. Knowledge of the high-pressure properties, however, is indispensable for a fundamental crystal-chemical understanding of ceramics under non-ambient conditions. For example, $M_2[Si_4N_6C]$ (M = Ho, Er) is stable to pressures of at least 36 GPa (Friedrich, Winkler *et al.*, 2005), while compounds like Si_3N_4 or $Ce_4[Si_4O_{3+x}N_{7+x}]Cl_{1-x}O_x$ (x = 0.12, 0.18, 0.2) transform to new high-pressure polymorphs at 15 and 8.6 GPa, respectively

(Zerr *et al.*, 1999; Friedrich, Knorr *et al.*, 2005; Friedrich *et al.*, 2006). The high-pressure behaviour of $Sr[SiAl_2O_3N_2]$, $Ce_4[Si_4O_4N_6]O$ and $Y_2[Si_4N_6C]$ was studied theoretically by quantum-mechanical calculations applying density functional theory up to 18, 18 and 30 GPa, respectively (Winkler *et al.*, 2001; Friedrich, Winkler *et al.*, 2005). No further high-pressure data on nitridosilicates and related compounds are known by the authors.

In this study we present results from *in situ* high-pressure X-ray powder diffraction of one nitridosilicate ($SrYb[Si_4N_7]$) and two sialons $MYb[Si_{4-x}Al_xO_xN_{7-x}]$ (x = 2; M = Sr, Ba) at pressures up to 42 GPa. The main objective of this work is to evaluate the influence of the substitution of Sr^{2+}/Ba^{2+} and $Si^{4+}N^{3-}/Al^{3+}O^{2-}$ on the compressibility.

2. Experimental

2.1. Synthesis

The $SrYb[Si_4N_7]$ sample was synthesized by Huppertz & Schnick (1997a). SrYb-sialon and BaYb-sialon were synthesized by high-temperature reaction in a radio-frequency furnace following the procedure described by Schnick *et al.* (1999). Chemical analysis was performed by electron microprobe analysis and a detailed description is given by Lieb (2006) and Lieb *et al.* (2005).

2.2. X-ray powder diffraction measurements

The $SrYb[Si_4N_7]$, SrYb- and BaYb-sialon powder samples were investigated at the ESRF at high pressures of up to 41, 42 and 37 GPa, respectively, using a LeToullec diamond–anvil cell with a gas-driven membrane for pressure generation (LeToullec *et al.*, 1988). Neon was loaded as the pressure-transmitting medium using an autoclave. Additionally, SrYb-sialon data up to 13 GPa were collected with nitrogen as the pressure-transmitting medium. Holes serving as sample chambers (approximately 150 μm in diameter) were drilled through inconel gaskets (pre-indented to a thickness of about 40 μm) using a spark-eroding drilling machine. Before and after each exposure, pressure was determined by the laser-induced ruby-fluorescence technique, applying the pressure scale of Mao *et al.* (1978). *In situ* high-pressure synchrotron X-ray powder diffraction data were collected at the ID9A high-pressure station at a wavelength of 0.4183 Å using a MAR345 online image-plate scanner. The sample-to-detector distance of 364 mm was determined from a Si reference sample. Diffraction data were collected at up to about $2\theta = 24°$ giving a maximum $\sin\theta/\lambda$ of 0.498 $Å^{-1}$.

The diffraction images were processed and integrated using *FIT2D* (Hammersley *et al.*, 1996). Intense and well defined single-crystal diffraction spots from individual larger grains of the sample, from the crystallized pressure medium, the diamonds and the rubies were masked manually and excluded from the integration. The integrated powder diffraction patterns were corrected for distortion by the image-plate scanner and the background was extracted using the program *DATLAB* (Syassen, 2005).

Figure 1
$SrYb[Si_4N_7]$ crystal structure: (*a*) layers of corner-sharing SiN_4 tetrahedra; (*b*) Si_6N_6-ring channels where $(Sr/Ba)^{2+}$ and Yb^{3+} ions are contained; (*c*) star-like $[N(SiN_3)_4]$ units and a chain of them. In the figures the silicon tetrahedra are drawn using different colours depending on the crystallographic site occupied [black for $Si_1(2a)$ and grey for $Si_2(6c)$].

Le Bail fits were performed using the program *FULLPROF* (Rodriguez-Carvajal, 2001) in order to obtain unit-cell parameters. As the SrYb- and BaYb-sialon compounds are isotypic with $SrYb[Si_4N_7]$, the starting parameters were taken from structural data published by Huppertz & Schnick (1997a). A linear interpolation between approximately 35 manually selected points for the background and a pseudo-Voigt profile function were used.

Equation-of-state (EOS) parameters of $SrYb[Si_4N_7]$, SrYb- and BaYb-sialon were determined by a least-squares fit of a third-order Birch–Murnaghan EOS (BM-EOS) using the program *EOS-FIT* (Angel, 1998). The volume at ambient pressure, V_0, the isothermal bulk modulus, B_0, and the first pressure derivative of the bulk modulus, B', were varied in the fit. All SrYb-sialon data were fitted by one EOS independent of the pressure-transmitting media used (Ne, N_2).

3. Results

Representative examples of the Le Bail fits at low and high pressure and their respective difference plots are shown in Fig. 2. The resulting unit-cell parameters of $SrYb[Si_4N_7]$, SrYb- and BaYb-sialon as a function of pressure are
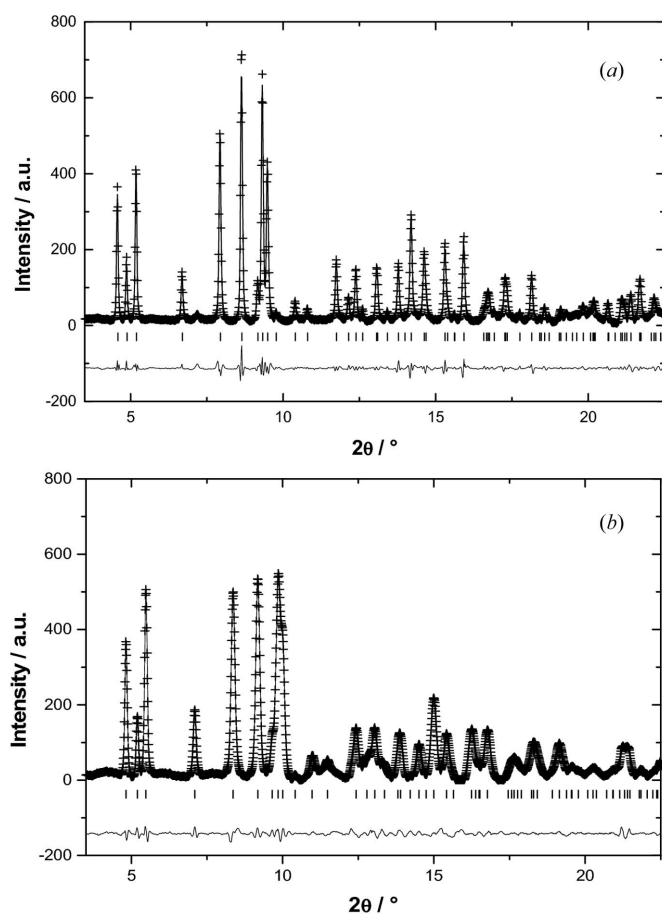
summarized in Tables 1, 2 and 3, respectively. The unit-cell parameters of $SrYb[Si_4N_7]$ obtained at ambient pressure agree with the data given by Huppertz & Schnick (1997a) within 3σ. No evidence for a pressure-induced structural phase transformation was observed, neither in $SrYb[Si_4N_7]$ nor in SrYb- or BaYb-sialon. The results of the EOS fits are shown in Table 4.

3.1. Bulk compressibility

The pressure dependence of the normalized volume (V/V_0) is plotted in Fig. 3. In order to make complex trends visible, which are not directly apparent from a p–V plot (Fig. 3), the volume–pressure data were transformed into an f–F, *i.e.* Eulerian strain *versus* normalized stress, plot (Angel, 2000). For a Birch–Murnaghan EOS the Eulerian strain is given by $f = 0.5[(V_0/V)^{2/3} - 1]$ and the normalized stress is defined as $F = p/[3f(1 + 2f)^{5/2}]$. The f–F plot gives a direct indication of the compression behaviour. If the data points lie on a horizontal line of constant F then $B' = 4$ and the data can be fitted with a second-order BM-EOS. If the data lie on an inclined straight line, the data will be adequately described by a third-order BM-EOS. Positive or negative slopes imply $B' > 4$ and $B' < 4$, respectively. In all of the cases the intercept on the F axis is the value of B_0 (Angel, 2000). The f–F plots of $SrYb[Si_4N_7]$, SrYb- and BaYb-sialon are shown in Fig. 4. The positive slopes in all data sets indicate that the pressure derivative of the bulk modulus is larger than 4, which implies that the use of a third-order BM-EOS is preferable to less complex functions.

While the slope of the BaYb-sialon p–V data appears similar to that of $SrYb[Si_4N_7]$ and SrYb-sialon in Fig. 4, the refined B' values are slightly different (Table 4). As can be seen in Fig. 4, the linear behaviour of the BaYb-sialon data becomes strongly non-linear at Eulerian strain values larger than around 0.045, which correspond to pressures higher than 30 GPa. Fitting a third-order BM-EOS to the BaYb-sialon data up to 30 GPa results in $V_0 = 317.3(5)$ $Å^3$, $B_0 = 168(2)$ GPa and $B' = 4.7(2)$, accompanied by a significant
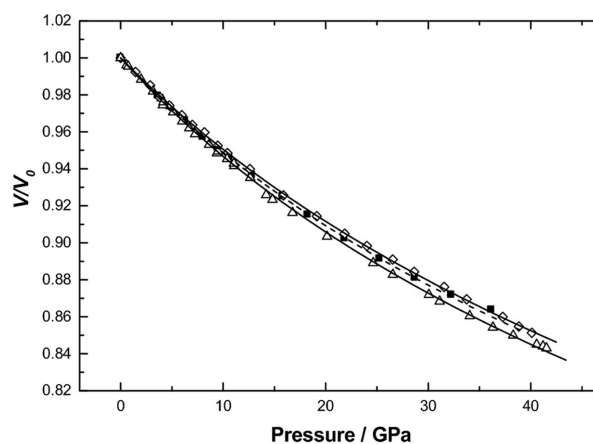
Figure 2
Observed (+), calculated (−), and the difference (at the bottom) X-ray powder diffraction profiles for SrYb-sialon at (*a*) 0.57 (1) and (*b*) 41.52 (5) GPa. Vertical marks correspond to the positions of the Bragg reflections.
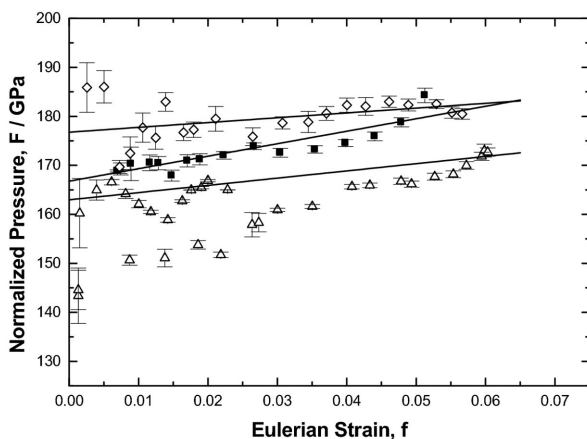
Figure 3
Variation of the normalized unit-cell volume *versus* pressure of $SrYb[Si_4N_7]$ (open diamonds), SrYb-sialon (open triangles) and BaYb-sialon (filled squares). EOS fits to data are represented by solid ($SrYb[Si_4N_7]$, SrYb-sialon) and dashed (BaYb-sialon) lines. Error bars are smaller than the symbol size ($B_0 = 4.7$ for BaYb-sialon).

Table 1
Pressure dependence of the unit-cell parameters of SrYb[Si$_4$N$_7$], space group $P6_3mc$.

p (GPa)	a (Å)	c (Å)	V (Å^3)
0.0001	5.9891 (3)	9.7511 (6)	302.91 (3)
1.44 (1)	5.9731 (8)	9.729 (1)	300.60 (7)
2.87 (1)	5.9594 (8)	9.702 (2)	298.41 (8)
3.82 (1)	5.9461 (7)	9.682 (1)	296.44 (6)
4.74 (3)	5.9367 (8)	9.669 (1)	295.11 (7)
5.95 (2)	5.9266 (9)	9.650 (2)	293.53 (9)
6.98 (2)	5.916 (1)	9.632 (2)	291.93 (9)
8.16 (2)	5.9048 (7)	9.613 (2)	290.78 (6)
9.46 (1)	5.894 (1)	9.592 (2)	288.54 (9)
10.41 (2)	5.8855 (9)	9.578 (2)	287.32 (8)
12.60 (5)	5.868 (1)	9.546 (2)	284.7 (1)
15.86 (6)	5.840 (1)	9.494 (2)	280.38 (9)
19.11 (1)	5.818 (1)	9.450 (3)	277.0 (1)
21.83 (8)	5.798 (1)	9.414 (2)	274.1 (1)
24.01 (5)	5.785 (1)	9.389 (2)	272.1 (1)
26.53 (3)	5.770 (1)	9.360 (3)	269.9 (1)
28.62 (9)	5.756 (1)	9.335 (3)	267.9 (1)
31.55 (3)	5.740 (1)	9.302 (3)	265.4 (1)
33.75 (3)	5.726 (1)	9.274 (3)	263.4 (1)
37.26 (1)	5.707 (1)	9.234 (2)	260.5 (1)
38.84 (3)	5.697 (1)	9.213 (3)	258.9 (1)
40.09 (3)	5.690 (2)	9.198 (3)	257.9 (1)

Figure 4
Volume–pressure data as a plot of the normalized pressure F against the Eulerian strain f of SrYb[Si$_4$N$_7$] (open diamonds), SrYb-sialon (open up-triangles) and BaYb-sialon (filled rectangles). EOS fits to data are represented by solid lines.

decrease of the e.s.d.s of B_0, B' and χ^2. The B' value obtained is similar to those of SrYb[Si$_4$N$_7$] and SrYb-sialon [B' = 4.4 (2) and 4.6 (2), respectively; Table 4]. Further studies are needed in order to clarify the origin of the non-linear behaviour above 30 GPa.

3.2. Linear compressibility

The pressure dependences of the normalized cell parameters (a/a_0 and c/c_0) and the axial ratios c/a of SrYbSi$_4$N$_7$, SrYb- and BaYb-sialon are plotted in Figs. 5 and 6, respectively. The compression of the a and c lattice parameters of BaYb-sialon is the same within error to the highest pressures studied (Figs. 5c and 6). A linear fit to the c/a data gives c/a = 1.62818 (6)–2 (5) × 10^{-5}p, where p is in GPa. Consequently, within the resolution of the experiment there is no p-depen-

Table 2
Pressure dependence of the unit-cell parameters of SrYb-sialon, space group $P6_3mc$.

p (GPa)	a (Å)	c (Å)	V (Å^3)
Pressure transmitting medium Ne			
0.0001	6.0420 (1)	9.820 (2)	310.5 (1)
0.57 (1)	6.034 (1)	9.807 (3)	309.2 (1)
4.10 (2)	5.992 (1)	9.731 (2)	302.5 (1)
6.68 (6)	5.965 (1)	9.671 (2)	298.06 (9)
9.38 (4)	5.938 (1)	9.627 (2)	293.94 (9)
11.07 (3)	5.921 (1)	9.589 (2)	291.17 (9)
14.19 (6)	5.895 (1)	9.552 (3)	287.4 (1)
14.81 (5)	5.890 (1)	9.542 (2)	286.7 (1)
16.76 (5)	5.875 (1)	9.515 (3)	284.5 (1)
20.12 (4)	5.850 (1)	9.464 (3)	280.5 (1)
24.62 (1)	5.821 (2)	9.407 (3)	276.0 (1)
26.54 (7)	5.808 (2)	9.381 (3)	274.1 (1)
30.06 (1)	5.787 (2)	9.335 (3)	270.7 (2)
31.11 (3)	5.780 (2)	9.319 (4)	269.6 (2)
34.04 (8)	5.763 (2)	9.287 (4)	267.1 (2)
36.31 (6)	5.751 (2)	9.260 (4)	265.2 (2)
38.27 (4)	5.742 (2)	9.241 (4)	263.9 (2)
40.59 (2)	5.733 (2)	9.217 (4)	262.3 (2)
41.19 (1)	5.731 (3)	9.213 (5)	262.0 (2)
41.52 (5)	5.729 (2)	9.207 (4)	261.7 (2)
Pressure transmitting medium N$_2$			
0.0001	6.0419 (8)	9.821 (2)	310.49 (8)
0.736 (1)	6.033 (1)	9.805 (2)	309.1 (1)
1.989 (3)	6.0186 (5)	9.782 (1)	306.86 (5)
3.144 (4)	6.0064 (6)	9.758 (1)	304.89 (6)
4.168 (1)	5.9947 (6)	9.738 (1)	303.07 (5)
5.123 (1)	5.9840 (6)	9.718 (1)	301.38 (5)
6.001 (8)	5.9743 (6)	9.701 (1)	299.85 (5)
7.257 (3)	5.9609 (6)	9.675 (1)	297.72 (5)
8.610 (8)	5.9487 (6)	9.656 (1)	295.92 (5)
9.479 (1)	5.9415 (6)	9.643 (1)	294.81 (6)
10.378 (1)	5.9343 (7)	9.626 (1)	293.56 (6)
11.030 (1)	5.9291 (6)	9.616 (1)	292.77 (6)
12.632 (3)	5.9141 (8)	9.587 (1)	290.38 (7)

Table 3
Pressure dependence of the unit-cell parameters of BaYb-sialon, space group $P6_3mc$.

p (GPa)	a (Å)	c (Å)	V (Å^3)
0.0001	6.083 (1)	9.904 (3)	317.3 (1)
3.64 (1)	6.042 (1)	9.834 (3)	310.8 (1)
3.91 (1)	6.038 (2)	9.830 (3)	310.4 (1)
4.75 (4)	6.029 (2)	9.816 (4)	309.0 (2)
6.30 (2)	6.013 (2)	9.790 (3)	306.6 (2)
7.01 (1)	6.006 (2)	9.778 (3)	305.5 (2)
8.00 (1)	5.995 (2)	9.760 (3)	303.8 (2)
9.49 (1)	5.982 (2)	9.739 (3)	301.8 (2)
10.61 (1)	5.972 (2)	9.721 (4)	300.2 (2)
12.82 (1)	5.952 (2)	9.689 (4)	297.3 (2)
15.81 (1)	5.927 (2)	9.649 (4)	293.6 (2)
18.25 (3)	5.906 (2)	9.614 (3)	290.4 (2)
21.85 (1)	5.878 (2)	9.570 (4)	286.4 (2)
25.26 (1)	5.854 (2)	9.530 (4)	282.9 (2)
28.70 (2)	5.832 (2)	9.493 (4)	279.6 (2)
32.26 (2)	5.812 (2)	9.459 (4)	276.7 (2)
36.19 (1)	5.795 (2)	9.427 (4)	274.1 (2)

dence of the c/a ratio in BaYb-sialon, but there may be a deviation from this behaviour above 35 GPa. To clarify this, further experiments at higher pressures are required. For SrYb[Si$_4$N$_7$] the linear compressibilities are equal, within errors, up to $\sim$ 10 GPa (Figs. 5a and 6). Above 10 GPa the c-axis becomes progressively more compressible. This beha-

Table 4
Parameters fitted with Birch–Murnaghan EOS.

	SrYb[Si$_4$N$_7$]	SrYb-sialon	BaYb-sialon	BaYb-sialon
V_0 (Å^3)	302.91 (6)	310.4 (1)	317.5 (2)	317.3 (5)
B_0 (GPa)	176 (2)	161 (2)	162 (3)	168 (2)
B'	4.4 (2)	4.6 (2)	5.4 (3)	4.7 (2)
χ^2	5.36	16.51	1.92	0.96
p_{max} (GPa)–pressure medium	41– Ne	42–N$_2$ + Ne	37–Ne	30–Ne
a_0 (Å)	5.9891 (3)	6.0421 (2)	6.084 (1)	
B_0 (GPa)	171 (2)	161 (2)	162 (3)	
B'	5.6 (1)	5.7 (2)	5.4 (3)	
χ^2	1.25	5.56	0.99	
p_{max} (GPa)–pressure medium	41–Ne	42–N$_2$ + Ne	37–Ne	
c_0 (Å)	9.7520 (8)	9.823 (3)	9.905 (1)	
B_0 (GPa	177 (2)	150 (4)	162 (3)	
B'	3.1 (1)	3.6 (1)	5.3 (4)	
χ^2	1.33	12.00	1.06	
p_{max}–pressure medium	41–Ne	42–N$_2$ + Ne	37–Ne	
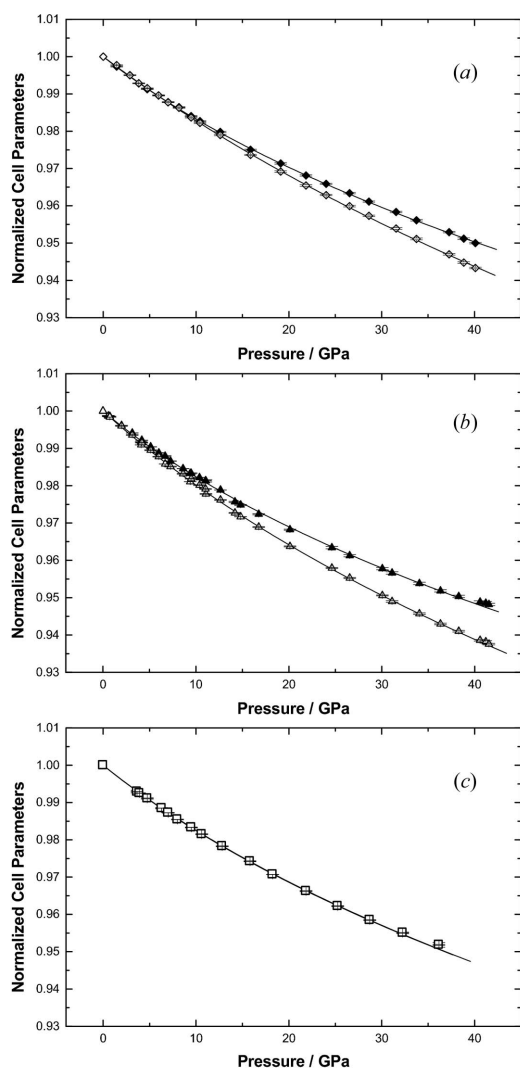
Figure 5
Variation of the normalized cell parameters [a/a_0 (filled symbols) and c/c_0 (open symbols)] of (a) SrYb[Si$_4$N$_7$], (b) SrYb-sialon and (c) BaYb-sialon as a function of pressure. As the compressibility of the a and c lattice parameters is essentially identical for BaYb-sialon, the data points are plotted on top of each other within curves. EOS fits to data are represented by solid lines.

viour, i.e. an increasing compressibility of the c-lattice parameter relative to the a-lattice parameter with increasing pressure, is even more pronounced in SrYb-sialon (Figs. 5b and 6). The variation of SrYb[Si$_4$N$_7$] and SrYb-sialon c/a data can be described by the polynomial equations $c/a = -5 \times 10^{-6}$ (6) $p^2 - 1 \times 10^{-4}$ (3) $p + 1.62900$ (4) and $c/a = -4.5 \times 10^{-6}$ (8) $p^2 - 3 \times 10^{-4}$ (3) $p + 1.6255$ (1), respectively (Fig. 6).

The linear incompressibilities (B_{0a}, B_{0c}) of SrYb[Si$_4$N$_7$], SrYb- and BaYb-sialon were obtained from a third-order BM-EOS fit to the pressure dependencies of the cube of the individual cell axes (Table 4). The Eulerian finite-strain analysis can be extended to obtain the compression behaviour of the a and c axes. Kruger et al. (1997) defined the strain parameters f_a and f_c for the a and c directions as well as the corresponding normalized pressures F_a and F_c in the following way: $f_a = 0.5[(a_0/a)^2 - 1]$; $f_c = 0.5[(c_0/c)^2 - 1]$; $F_a = p(ac_0/a_0c)^{2/3}/[f_a(1 + 2f_v)^{2.5}]$; and $F_c = p(a_0c/ac_0)^{4/3}/[f_c(1 + 2f_v)^{2.5}]$, where f_v is the Eulerian volume strain. The linear incompressibilities provide a quantitative measure of the degree to which the compression is isotropic. They are related to the hexagonal bulk modulus by $1/B_0 = 2/B_{0a} + 1/B_{0c}$. The f_a–F_a and f_c–F_c plots are shown in Fig. 7.

The compressibility of the a-axis is similar for all of these compounds and is represented by a positive slope in the f_a–F_a plots. Contrary, the c-axes compress differently as can be seen in Fig. 7 and Table 4. Similar to the p–V data, the f_a–F_a and f_c–F_c plots of BaYb-sialon become strongly non-linear at Eulerian strain values higher than around 0.045, which correspond to pressures higher than 30 GPa.

4. Discussion

The variation of the unit-cell parameters and volume of isotypic compounds like MYb[Si$_4$N$_7$] (M = Eu, Sr, Ba;
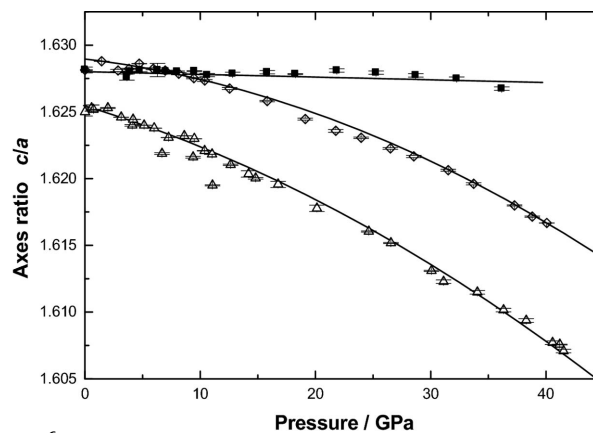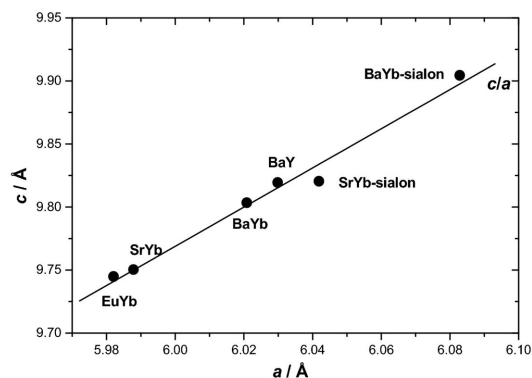

Figure 6
Variation of the axes ratio c/a versus pressure of SrYb[Si$_4$N$_7$] (open diamonds), SrYb-sialon (open up-triangles) and BaYb-sialon (filled rectangles). Linear (BaYb-sialon) and second-order polynomial (SrYbSi$_4$N$_7$ and SrYb-sialon) fits to data are represented by solid lines.
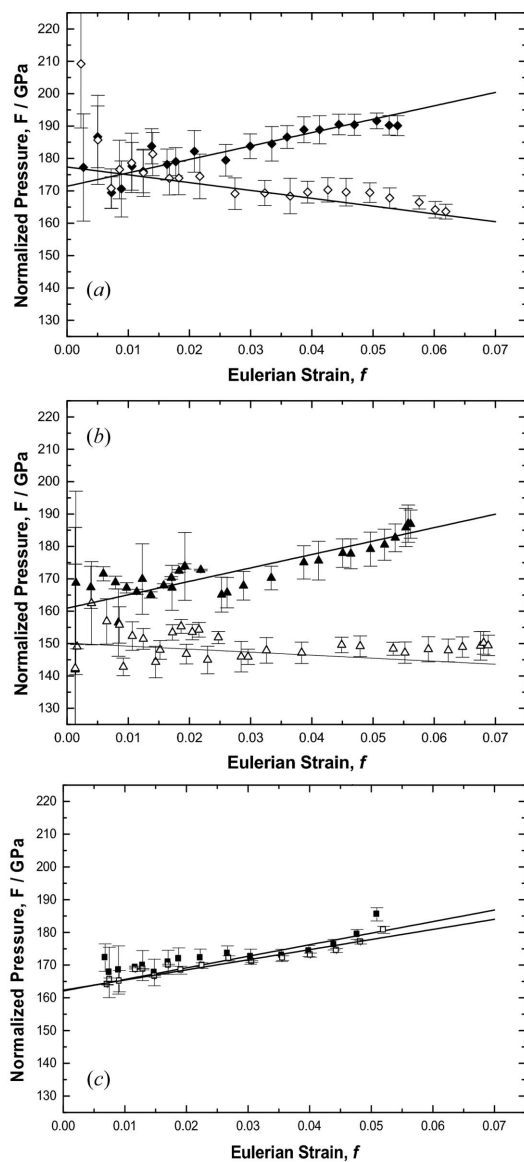
Figure 7
The pressure dependencies of the cell parameters [*a* (filled symbols) and *c* (open symbols)] are plotted as a normalized pressure *F* against the Eulerian strain *f* of (*a*) SrYb[Si$_4$N$_7$], (*b*) SrYb-sialon and (*c*) BaYb-sialon. EOS fits to data are represented by solid lines.

Huppertz & Schnick, 1997*a*,*b*), BaY[Si$_4$N$_7$] (Fang *et al.*, 2003), SrYb- and BaYb-sialon under ambient conditions can be rationalized in terms of the substitution in the individual sublattices (Fig. 8). The exchange of the metal cations, where Ba^{2+} (1.61 Å) and Sr^{2+} (1.44 Å) replace Eu^{2+} (1.35 Å), and Y^{3+} (0.9 Å) replaces Yb^{3+} (0.868 Å)[1], can be described by the same systematic structural change as the coupled substitution, where Al^{3+} (0.39 Å) replaces Si^{4+} (0.26 Å), while O^{2-} (1.38 Å) replaces N^{3-} (1.46 Å). These substitutions do not significantly influence the *c*/*a* ratios, whose values remain approximately constant at around 1.63. Hence, in all compounds the incorporation of larger ions expands the *c* axis (1.63) as much as the *a* axis.

---

[1] Ionic radii were taken from Shannon (1976).

Figure 8
Variation in the unit-cell parameters of the isotypic compounds *M*Yb[Si$_4$N$_7$] (*M* = Eu, Sr, Ba), BaY[Si$_4$N$_7$], SrYb- and BaYb-sialon at room pressure. A linear fit to the data is represented by a solid line. The *c*/*a* value is almost constant at around 1.63.

In general, a comparison of the isothermal bulk modulus indicates that SrYb[Si$_4$N$_7$] [B_0 = 176 (2) GPa] is less compressible than SrYb-sialon [B_0 = 161 (2) GPa] and BaYb-sialon [B_0 = 168 (2) GPa], sialons being more compressible than nitridosilicates. The Si^{4+}N^{3-}/Al^{3+}O^{2-} tetrahedral network substitution has a larger effect on compressibility than the Ba/Sr substitution, which shows that the overall compressibility is not dominated by the size of the substituted cations but by the compression of the tetrahedral network.

The values for B_0 and B' obtained in this work are of a comparable magnitude with those found in the structurally related nitridocarbidosilicates M_2[Si$_4$N$_6$C] (*M* = Ho, Er) with B_0 equal to 162 (2) and 163 (4) GPa, respectively (Friedrich, Winkler *et al.*, 2005). The nitridocarbidosilicates exhibit C$^{[4]}$ links comparable with the N$^{[4]}$ links of the title compounds. The sialon SrSi[Al$_2$O$_3$N$_2$], the oxonitridosilicate oxide Ce$_4$Si$_4$O$_4$N$_6$O and the isotypic chloride Ce$_4$[Si$_4$O$_{3+x}$N$_{7+x}$]Cl$_{1-x}$O$_x$ (*x* = 0.12, 0.18), which do not exhibit N$^{[4]}$ links in the crystal structure but only O$^{[2]}$ and N$^{[2]}$ links, are much more compressible, with B_0 = 131.9 (3), 131 (2), 124 (5) and 153 (10) GPa for the low- and high-pressure polymorph, respectively (Winkler *et al.*, 2001; Friedrich, Knorr *et al.*, 2005). Hence, the presence of N$^{[4]}$ or C$^{[4]}$ links decreases the compound's compressibility compared with compounds that only show O$^{[2]}$ and N$^{[2]}$ links, because the star-like [A(SiN$_3$)$_4$] (*A* = N, C) units generate a stiff three-dimensional framework. This can further explain the unusually high stability of these silicates at pressures up to at least 42 GPa. No O$^{[4]}$ links are known as yet, which prevents a direct comparison between the compressibilities of the title compound with related oxosilicates, as these are strongly varying with the crystal structure.

The axial compressibility indicates that, at least for SrYb[Si$_4$N$_7$] and SrYb-sialon, the *c*-axis becomes more compressible than the *a*-axis with increasing pressure. This behaviour can be related to the occurrence of layers of corner-sharing SiN$_4$ tetrahedra, which are arranged perpendicular to the *c* axis (Fig. 1). Thus, the structure is relatively stiff within the strongly connected layers owing to the repulsive forces of ions that become stronger at decreasing distances. The corner-sharing SiN$_4$ tetrahedra that join the layers along the *c* axis

have more freedom for displacement or distortion along [001], hence favouring the compression.

In contrast to $SrYb[Si_4N_7]$ and SrYb-sialon, in BaYb-sialon the compression of the *a*- and *c*-lattice parameters is almost equal. This could be due to the Sr^{2+}/Ba^{2+} substitution. Since the exchanged ions have bigger ionic radii, the polyhedral arrangement becomes less stiff, hence allowing more compression within the (001) layers. The onset of nonlinear behaviour observed around 30 GPa might be the beginning of a similar behaviour to that observed in $SrYb[Si_4N_7]$ and SrYb-sialon where the *c*-lattice parameter is more compressible than the *a*-axis parameters.

In summary, this study presents the first experimentally determined compressibilities of a nitridosilicate, $SrYb[Si_4N_7]$, and of two oxonitridoaluminosilicates, $MYb[Si_{4-x}Al_xO_xN_{7-x}]$, $x = 2$ and M = Sr, Ba. Further experiments at even higher pressures are needed in order to clarify whether the deviations from the low-pressure behaviour are indicative of an approach to the limit of phase stability. Higher resolution or single-crystal experiments, or parameter-free modelling studies are required to determine the compression mechanism. Such studies are currently underway by our group and, in conjunction with the present study, will serve as a basis for the understanding of the pressure dependence of the structure–property relationships of this class of compounds.

References

Amutha Rani, D., Yoshizawa, Y., Jones, M. I., Hyuga, H., Hirao, K. & Yamauchi, Y. (2005). *J. Am. Ceram. Soc.* **88**, 1655–1658.

Angel, R. (1998). *EOS-FIT.* Version 4.2.

Angel, R. (2000). *High-Pressure and High-Temperature Crystal Chemistry; MSA Reviews in Mineralogy and Geochemistry*, edited by R. M. Hazen & R. T. Down, Vol. 41, pp. 35–60.

Fang, C. M., Li, Y. Q., Hintzen, H. T. & de With, G. (2003). *J. Mater. Chem.* **13**, 1480–1483.

Friedrich, A., Haussühl, E., Morgenroth, W., Lieb, A., Winkler, B., Knorr, K. & Schnick, W. (2006). *Acta Cryst.* B**62**, 205–211.

Friedrich, A., Knorr, K., Lieb, A., Rath, S., Hanfland, M., Winkler, B. & Schnick, W. (2005). *Z. Kristallogr.* **220**, 245–249.

Friedrich, A., Winkler, B. & Knorr, K. (2005). *Z. Kristallogr.* Suppl. 22, 88.

Hammersley, A. P., Svensson, S. O., Hanfland, M., Fitch, A. N. & Häusermann, D. (1996). *High Press. Res.* **14**, 235–248.

Häntsche, J. P. & Spicher, U. (2005). *Mater.-Wiss. u. Werkstofftech.* **36**, 108–116.

Haviar, M., Lences, Z. & Herbertsson, H. (1997). *J. Mater. Sci. Lett.* **16**, 236–238.

Huppertz, H. & Schnick, W. (1997*a*). *Z. Anorg. Allg. Chem.* **623**, 212–217.

Huppertz, H. & Schnick, W. (1997*b*). *Acta Cryst.* C**53**, 1751–1753.

Jack, K. H. & Wilson, W. I. (1972). *Nature (London)*, **238**, 128–129.

Kruger, M. B., Nguyen, J. H., Li, Y. M., Caldwell, W. A., Manghnami, M. H. & Jeanloz, R. (1997). *Phys. Rev. B*, **55**, 3456–3460.

Lauterbach, R., Irran, E., Henry, P. F., Weller, M. T. & Schnick, W. (2000). *J. Mater. Chem.* **10**, 1357–1364.

LeToullec, R., Pinceaux, J. P. & Loubeyre, P. (1988). *High Press. Res.* **1**, 77–90.

Lieb, A. (2006). PhD thesis, Ludwig Maximilians Universität, Munich, Germany.

Lieb, A., Weller, M. T., Henry, P. F., Niewa, R., Pöttgen, R., Hoffmann, R. D., Höfer, H. E. & Schnick, W. (2005). *J. Solid State Chem.* **178**, 976–988.

Mao, H., Bell, P., Shaner, J. & Steinberg, D. (1978). *J. Appl. Phys.* **49**, 3276–3283.

Rodriguez-Carvajal, J. (2001). *FullProf.* Version 1.9c. LLB, CEA/Saclay, France.

Shannon, R. D. (1976). *Acta Cryst.* A**32**, 751–767.

Schnick, W. (1993). *Angew. Chem. Int. Ed. Engl.* **32**, 806–818.

Schnick, W. (2001). *Int. J. Inorg. Mater.* **3**, 1267–1272.

Schnick, W., Huppertz, H. & Lauterbach, R. (1999). *J. Mater. Chem.* **9**, 289–296.

Syassen, K. (2005). *DATLAB.* Version 1.37d. MPI/FKF Stuttgart, Germany.

Winkler, B., Hytha, M., Hantsch, U. & Milman, V. (2001). *Chem. Phys. Lett.* **343**, 622–626.

Zerr, A., Miehe, G., Serghiou, G., Schwarz, M., Kroke, E., Riedel, R., Fueß, H., Kroll, P. & Boehler, R. (1999). *Nature (London)*, **400**, 340–342.